




Majorana spin current generation by dynamic strain

Yuki Yamazaki ¹, Takumi Funato ^{2,3}, and Ai Yamakage ¹

¹Department of Physics, Nagoya University, Nagoya 464-8602, Japan

²Center for Spintronics Research Network, Keio University, Yokohama 223-8522, Japan

³Kavli Institute for Theoretical Sciences, University of Chinese Academy of Sciences, Beijing 100190, People's Republic of China



(Received 12 January 2023; accepted 31 July 2023; published 17 August 2023)

Majorana fermions that emerge on the surface of topological superconductors are charge neutral but can have higher-rank electric multipoles by allowing for time-reversal and crystalline symmetries. Applying the general classification of these multipoles, we show that the spin current of Majorana fermions is driven by spatially nonuniform dynamic strains on the surface of a 3D topological crystalline superconductor. We find that the frequency dependence of the Majorana spin current reflects the energy dispersion of Majorana fermions. Our results provide new dynamics of Majorana fermions characterized by crystalline and superconducting symmetries.

DOI: [10.1103/PhysRevB.108.L060505](https://doi.org/10.1103/PhysRevB.108.L060505)

Majorana fermions (MFs) are charge-neutral relativistic particles moving in 3D space. In addition, two types of MFs emerge in topological superconductors (TSCs) as gapless Andreev bound states [1–7]. One type is a spatially localized zero-dimensional MF, which appears at the ends of nanowires [8–14] or in the cores of the vortices of TSCs [15–18]. MFs have been the subject of considerable research because of their potential application to fault-tolerant topological quantum computation with non-Abelian statistics [19,20].

Here, one can ask the following question: what are the physical phenomena unique to spatially extended 1D or 2D MFs? A typical example is the half-integer thermal quantum Hall effect on the surface of a TSC [21–23]. “Half-Integer” is a peculiarity originating from the fact that MFs are heat carriers. The half-integer thermal quantum Hall effect is unique to MFs that are spread in 2D space, and its “driving force” is a thermal gradient. Recently, the optical response of Majorana chiral edge modes has also been discussed [24,25]. The frequency dependence of the real part of the optical conductivity is proportional to ω^2 , through which these modes can be distinguished from trivial superconductors or insulators and Dirac chiral edge modes. Then, the driving force of MFs is an electromagnetic wave. In superconductors, the responses to acoustic waves have been extensively studied through ultrasonic attenuation measurements [26,27] to investigate the superconducting symmetry or measurements of the temperature dependence of the superconducting gap [28]. Therefore, we can expect to be able to use dynamic strains for the driving force of MFs on the surfaces of 3D TSCs.

When MFs have time-reversal symmetry, they do not appear alone but form Kramers pairs, which are called Majorana Kramers pairs (MKPs). Due to the time-reversal symmetry, a single MKP is stable against an external electric field. Previously, we derived the general effective theory for the electromagnetic properties of “double” MKPs on the surface of a 3D TSC [29–31]. Double MKPs can have various electric multipole degrees of freedom that are qualitatively different from those of ordinary fermions, and it has been shown that

they can respond to static strains [31]. Double MKPs are always protected by crystalline symmetries in addition to time-reversal symmetry; thus, TSCs are specifically referred to as topological crystalline superconductors (TCSCs).

In this Letter, we clarify the transport phenomena of double MKPs driven by spatially nonuniform dynamic strains on the surface of 3D TCSCs. We start with a 4×4 Dirac Hamiltonian with respect to the surface point group (PG) symmetry. Then, we reveal the spin current of double MKPs, referred to as the “Majorana spin current,” generated by spatially nonuniform dynamic strains on the surface (see Fig. 1). When there is no gap in the dispersion of double MKPs, we find that the Majorana spin current is caused by an intrinsic

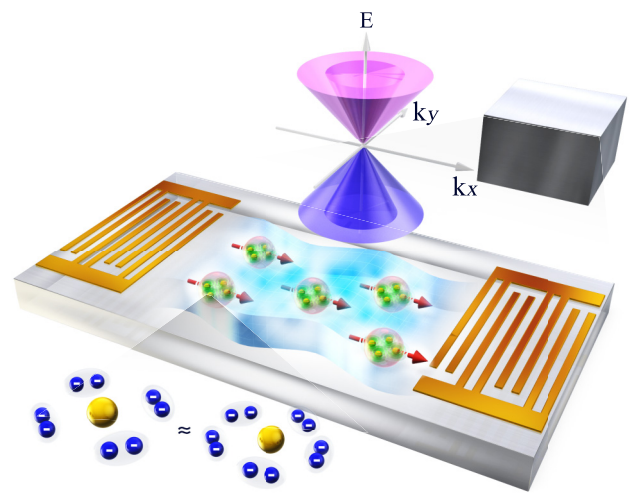


FIG. 1. Schematic showing that Majorana spin currents flow on the surface of a 3D TCSC driven by a dynamic strain. The surface has four Majorana fermions that form double MKPs. Double MKPs have electric quadrupoles coupled to a dynamic strain, and the spin current of Majorana electric quadrupoles is generated by a dynamic strain.

effect and does not depend on the relaxation time. Alternatively, for the gapped case induced by surface magnetization, the Majorana spin current has two frequency regions that reflect the energy dispersion of double MKPs. Our results provide new dynamics of Majorana fermions characterized by crystalline and superconducting symmetries, and accelerate the study of the coupling of given external fields with MFs and the resulting transport phenomena.

Before we consider the main topic, we discuss the electromagnetic properties of MKPs on the surface of a TSC. When there is only one MF on the surface, the single MF is strongly protected by particle-hole symmetry (charge-neutrality constraint), and it is extremely stable against any external fields. If a TSC has time-reversal symmetry, then two MFs form an MKP. The single MKP is protected by time-reversal symmetry, and hence, it generally responds only to external magnetic fields and remains stable to external electric fields. On the other hand, when crystalline symmetries are taken into account, double MKPs can exist, and they can respond to an electrical perturbation that breaks the crystalline symmetry. The coupling of N MKPs to a spatially uniform external field can be represented according to Ref. [31] by

$$\hat{H}_{\text{surf,ex}} = -\hat{O}F, \quad \hat{O} = \frac{1}{2} \int d^2x \sum_{ss'} \hat{\psi}_s(\mathbf{x})(A_F)_{ss'} \hat{\psi}_{s'}(\mathbf{x}), \quad (1)$$

where $\hat{\psi}_s(\mathbf{x})$ ($s = 1, \dots, 2N$) are Majorana field operators and satisfy $\hat{\psi}_s^\dagger(\mathbf{x}) = \hat{\psi}_s(\mathbf{x})$. A_F is conjugate to F and should be an antisymmetric Hermite matrix since Majorana field operators obey $\{\hat{\psi}_s(\mathbf{x}), \hat{\psi}_{s'}(\mathbf{x}')\} = \delta_{ss'} \delta^2(\mathbf{x} - \mathbf{x}')$. When A_F is the 2×2 matrix with only one MKP, there exists only $A_F = \sigma_y$ satisfying $\Theta_{\text{surf}} A_F \Theta_{\text{surf}}^{-1} = -A_F$ for the time-reversal operator $\Theta_{\text{surf}} = (-i\sigma_y K)$. K is a complex conjugation, and hence, the MKP couples only to external magnetic fields. On the other hand, when A_F is the 4×4 matrix with double MKPs, A_F satisfying $\Theta_{\text{surf}} A_F \Theta_{\text{surf}}^{-1} = A_F$ can be formed, and the double MKPs can also be coupled to an external electric field according to Eq. (1). Double MKPs have various electric multipoles depending on the crystalline symmetry of the surface, i.e., wallpaper groups (WGs), and superconducting symmetry. In a previous study [31], we revealed the coupling between the electric multipoles and spatially uniform static strain for each WG. In the following, we first show that dynamic strains generate a finite spin current by using a concrete model based on the symmetries of the system. Then, we discuss the general theory of couplable strains and the resulting surface spin currents, depending on the crystalline and superconducting symmetries of the system.

We consider the 3D time-reversal-invariant topological superconductor with O_h PG symmetry, which belongs to the A_{1u} superconducting state. Then, we utilize the low-energy model for double MKPs on the (001) surface with the $p4m$ WG symmetry, which equals the C_{4v} PG symmetry. The surface symmetry operations are given by $D_{\{C_{4z}|0\}} = \frac{-1}{\sqrt{2}}(s_0\tau_3 - is_3\tau_3)$ and $D_{\{\sigma_{(xz)}|0\}} = \frac{i}{\sqrt{2}}(s_2\tau_3 - s_1\tau_3)$, with D_g being a representation matrix of $g \in C_{4v}$, where $s_i\tau_j$'s are the product of Pauli matrices acting on the spin, orbital, and sublattice degrees of freedom. The time-reversal Θ , particle-hole C , and chiral Γ symmetries are also defined by $\Theta = s_2\tau_3K$, $C = s_1\tau_0K$, and $\Gamma = s_3\tau_3$. We note that these representations of surface sym-

metry operations are determined by the bulk superconducting symmetry [30,31] (see Sec. I of the Supplemental Material [32]). Then, we obtain the total symmetric Hamiltonian:

$$\hat{H} = \frac{1}{2} \sum_{\mathbf{k}} \hat{\psi}_{\mathbf{k}}^\dagger H(\mathbf{k}) \hat{\psi}_{\mathbf{k}},$$

$$H(\mathbf{k}) = [v_1(\eta_1 k_y - \eta_2 k_x) + v_2(\eta_3 k_y - \eta_4 k_x)], \quad (2)$$

where $\hat{\psi}_{\mathbf{k}}^\dagger = (\hat{\psi}_{1\mathbf{k}}^\dagger, \hat{\psi}_{2\mathbf{k}}^\dagger, \hat{\psi}_{3\mathbf{k}}^\dagger, \hat{\psi}_{4\mathbf{k}}^\dagger)$ and $\hat{\psi}_{\mathbf{k}} = {}^t(\hat{\psi}_{1\mathbf{k}}, \dots, \hat{\psi}_{4\mathbf{k}})$ are the Majorana creation/annihilation operators, which satisfy $\hat{\psi}_{1\mathbf{k}}^\dagger = \hat{\psi}_{2-\mathbf{k}}$ and $\hat{\psi}_{3\mathbf{k}}^\dagger = \hat{\psi}_{4-\mathbf{k}}$, and the subscripts 1, ..., 4 denote four MFs. The η_i 's are given by $\eta_1 = (1/\sqrt{2})(s_1\tau_0 + s_2\tau_0)$, $\eta_2 = (-1/\sqrt{2})(s_1\tau_0 - s_2\tau_0)$, $\eta_3 = (1/\sqrt{2})(s_1\tau_3 + s_2\tau_3)$, and $\eta_4 = (-1/\sqrt{2})(s_1\tau_3 - s_2\tau_3)$. $H(\mathbf{k})$ satisfies $\Theta H(\mathbf{k}) \Theta^{-1} = H(-\mathbf{k})$, $CH(\mathbf{k})C^{-1} = -H(-\mathbf{k})$, $\Gamma H(\mathbf{k})\Gamma^{-1} = -H(\mathbf{k})$, and $D_g H(\mathbf{k}) D_g^\dagger = H(g\mathbf{k})$, where a momentum \mathbf{k} is transformed to $g\mathbf{k}$ under the action of g . The spin of MFs is represented by $\boldsymbol{\sigma} = (\sigma_x, \sigma_y, \sigma_z) \equiv (\eta_5, \eta_6, -s_3\tau_0)$, where $\eta_5 = (1/\sqrt{2})(s_1\tau_2 - s_2\tau_2)$ and $\eta_6 = (-1/\sqrt{2})(s_1\tau_2 + s_2\tau_2)$, which are coupled to the magnetization \mathbf{M} as $\mathbf{M} \cdot \boldsymbol{\sigma}$. In this model, the double MKPs have specific electromagnetic multipoles with particle-hole symmetry; the double MKPs have magnetic multipoles that are represented by $\boldsymbol{\sigma}$ and electric quadrupoles that are represented by $s_3\tau_1$ with the B_1 representation and $s_0\tau_2$ with the B_2 representation. Therefore, in the following, we can define the spin currents $j_x^y + j_y^x$ and $j_x^x - j_y^y$ generated by dynamic strains $u_{xx} - u_{yy}$ and $u_{xy} + u_{yx}$, where $u_{ij}(\mathbf{x}) = \partial_i u_j(\mathbf{x})$ and $u_j(\mathbf{x}) \propto e^{i(\mathbf{q} \cdot \mathbf{x} - \omega t)}$ denote the displacement fields (Fig. 1). The spin current is defined by $j_i^\alpha \equiv \frac{1}{2} \langle \sigma_\alpha, \partial H(\mathbf{k}) / \partial k_i \rangle$ ($i = x, y$), which satisfies particle-hole symmetry $C j_i^\alpha C^{-1} = -j_i^\alpha$. Then, we obtain $\hat{j}_y^x(\mathbf{q}) + \hat{j}_x^y(\mathbf{q}) = \frac{1}{2} \sum_{\mathbf{k}} \hat{\psi}_{\mathbf{k}-\frac{\mathbf{q}}{2}}^\dagger [-v_2 s_3 \tau_1] \hat{\psi}_{\mathbf{k}+\frac{\mathbf{q}}{2}}$ and $\hat{j}_x^x(\mathbf{q}) - \hat{j}_y^y(\mathbf{q}) = \frac{1}{2} \sum_{\mathbf{k}} \hat{\psi}_{\mathbf{k}-\frac{\mathbf{q}}{2}}^\dagger [v_1 s_0 \tau_2] \hat{\psi}_{\mathbf{k}+\frac{\mathbf{q}}{2}}$.

Here, we define the electrical operators, which are represented by $\hat{O}^{(1)}(\mathbf{q}) \equiv \frac{1}{2} \sum_{\mathbf{k}} \hat{\psi}_{\mathbf{k}-\frac{\mathbf{q}}{2}}^\dagger (\rho_1 s_3 \tau_1) \hat{\psi}_{\mathbf{k}+\frac{\mathbf{q}}{2}}$ and $\hat{O}^{(2)}(\mathbf{q}) \equiv \frac{1}{2} \sum_{\mathbf{k}} \hat{\psi}_{\mathbf{k}-\frac{\mathbf{q}}{2}}^\dagger (\rho_2 s_0 \tau_2) \hat{\psi}_{\mathbf{k}+\frac{\mathbf{q}}{2}}$. Since $\hat{O}^{(1)}$ and $u_{xx} - u_{yy}$ as well as $\hat{O}^{(2)}$ and $u_{xy} + u_{yx}$ share the same representation, the couplings between double MKPs and the dynamic strains are represented by

$$\hat{H}_{\text{surf,ex}} = -\{\hat{O}^{(1)}(\mathbf{q})[u_{xx}(\mathbf{q}, \omega) - u_{yy}(\mathbf{q}, \omega)] + \hat{O}^{(2)}(\mathbf{q})[u_{xy}(\mathbf{q}, \omega) + u_{yx}(\mathbf{q}, \omega)]\}. \quad (3)$$

Then, we calculate the linear response of the spin currents $\hat{j}_y^x + \hat{j}_x^y$ and $\hat{j}_x^x - \hat{j}_y^y$ to the dynamic strains given by Eq. (3):

$$\langle \hat{j}_y^x + \hat{j}_x^y \rangle(\mathbf{q}, \omega) \equiv K_1(\mathbf{q}, \omega)[u_{xx}(\mathbf{q}, \omega) - u_{yy}(\mathbf{q}, \omega)] + K_2(\mathbf{q}, \omega)[u_{xy}(\mathbf{q}, \omega) + u_{yx}(\mathbf{q}, \omega)], \quad (4)$$

$$\langle \hat{j}_x^x - \hat{j}_y^y \rangle(\mathbf{q}, \omega) \equiv K_1'(\mathbf{q}, \omega)[u_{xx}(\mathbf{q}, \omega) - u_{yy}(\mathbf{q}, \omega)] + K_2'(\mathbf{q}, \omega)[u_{xy}(\mathbf{q}, \omega) + u_{yx}(\mathbf{q}, \omega)], \quad (5)$$

where the response function $K_i(\mathbf{q}, \omega)$ is given in Ref. [33] as

$$K_i(\mathbf{q}, \omega) \equiv i \int_0^\infty dt e^{i(\omega+i\delta)t} \langle [\hat{j}_y^x(\mathbf{q}, t) + \hat{j}_x^y(\mathbf{q}, t), \hat{O}^{(i)}(-\mathbf{q}, 0)] \rangle, \quad (6)$$

where $\hat{A}(t) = e^{i\hat{H}t}\hat{A}e^{-i\hat{H}t}$ and $\delta \rightarrow +0$. $K'_i(\mathbf{q}, \omega)$ is also defined by replacing $\hat{j}_x^y + \hat{j}_y^x$ with $\hat{j}_x^x - \hat{j}_y^y$ in Eq. (6). Note that the chemical potential μ for MFs is equal to zero due to the particle-hole symmetry in superconducting states. Additionally, $\langle \dots \rangle = \text{tr}[e^{-\hat{H}/T} \dots] / \text{tr}[e^{-\hat{H}/T}]$. If there are no applied external fields, then $K_1(\mathbf{q}, \omega)$ and $K'_2(\mathbf{q}, \omega)$ only take finite values since the spin currents and dynamic strains share the same representation of C_{4v} . Here, we assume that the wave number q and the frequency ω are smaller than the mean free path l and relaxation time τ of the MFs. These conditions are represented by $q \ll l^{-1}$ and $\omega \ll \tau^{-1} = 2\gamma$, where γ is the impurity scattering [34]. We expand the response function for ω and consider the nonequilibrium part: $K_i(\omega) - K_i(0)$ (the details are shown in Sec. II of the Supplemental Material [32]):

$$K_1(\omega) - K_1(0) \simeq \frac{i\omega}{8\pi^2} \frac{\rho_1}{v_1} \ln \left[\frac{(v_1 - v_2)^2}{(v_1 + v_2)^2} \right]. \quad (7)$$

One can see that $K_1(\omega) - K_1(0)$ does not depend on γ . Such independence from impurity scattering for a system with linear dispersion also occurs in the minimal conductivity problem of graphene [35]. We note that $K'_2(\omega) - K'_2(0) = \frac{v_1\rho_2}{-v_2\rho_1}(K_1(\omega) - K_1(0))$ because of the chiral symmetry.

Next, we consider the case in which the dispersion of double MKPs is gapped. This situation can be realized, for example, by attaching ferromagnets on the surface. Then, the effective Hamiltonian is given by

$$\tilde{H}(\mathbf{k}) = H(\mathbf{k}) + \tilde{M}_z \sigma_z. \quad (8)$$

The second term in Eq. (8) is the Zeeman term reflected by the coupling between the spin moment of double MKPs and the magnetization of ferromagnets, where we define $M_z \equiv -\tilde{M}_z$. Then, the energy dispersion is given by $E_{\tau=\pm, \pm} = \pm \sqrt{M_z^2 + k^2(v_1 + \tau v_2)^2}$. The applied magnetization opens an energy gap in the dispersion of double MKPs and lowers the symmetry from C_{4v} to C_4 . Therefore, $K_2(\omega)$ can take a finite value since $j_y^x + j_x^y$ and $u_{xy} + u_{yx}$ share the same irreducible representation of C_4 . The relationship between B_z and ω is important; hence, we calculate the response function by using the Lehmann representation:

$$K_i(\omega) = \frac{1}{4} \sum_{n \in \text{occ}, m \in \text{unocc}} \left\{ \frac{\langle n | -v_2 s_3 \tau_1 | m \rangle \langle m | o^{(i)} | n \rangle}{E_n - E_m + \omega + i\delta} + \left[\frac{\langle n | -v_2 s_3 \tau_1 | m \rangle \langle m | o^{(i)} | n \rangle}{E_n - E_m - \omega + i\delta} \right]^* \right\}, \quad (9)$$

$$o^{(1)} = \rho_1 s_3 \tau_1, \quad o^{(2)} = \rho_2 s_0 \tau_2,$$

where $\delta \rightarrow +0$ and $|n\rangle$ and $|m\rangle$ denote the occupied states and unoccupied states of Eq. (8), respectively. As a result, we obtain the nonequilibrium part: $K_i(\omega) - K_i(0)$:

$$K_1(\omega) - K_1(0) = \begin{cases} A \frac{\omega^2}{M_z^2} & (\omega \ll 2|M_z|), \\ B \left(-\frac{\omega}{2} \ln \left| \frac{1 + \frac{2k_c v_1}{\omega}}{1 - \frac{2k_c v_1}{\omega}} \right| + \frac{2M_z v_1^2}{v_1^2 - v_2^2} - \frac{M_z v_1 \ln \left| \frac{v_1 - v_2}{v_1 + v_2} \right|}{2v_2} \right) + i \frac{B\pi v_1}{2v_2} \omega & (2|M_z| \ll \omega \ll x(k_c)), \end{cases} \quad (10)$$

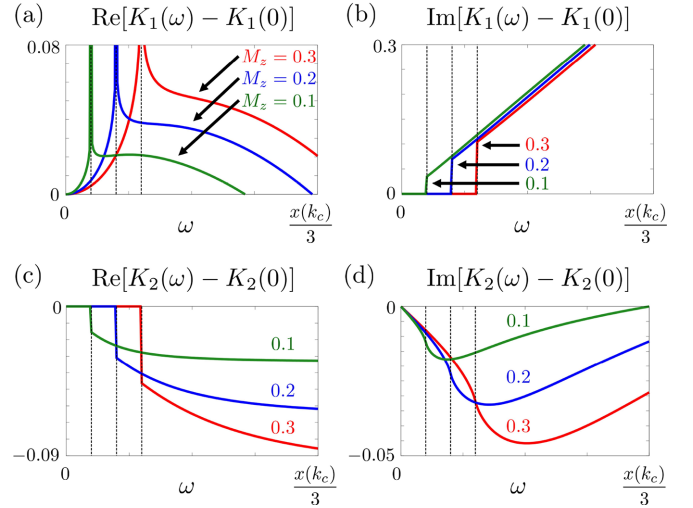


FIG. 2. Numerical results of (9). (a) and (b) show the amplitudes of the real and imaginary parts of $K_1(\omega) - K_1(0)$, respectively. (c) and (d) show the real and imaginary parts of $K_2(\omega) - K_2(0)$, respectively. Red, blue, and green lines denote the cases of $|M_z| = 0.3$, $|M_z| = 0.2$ and $|M_z| = 0.1$, respectively. The values of the three black dotted lines drawn on the horizontal axis in (a), (b), (c), and (d) denote the size of the energy gap $2|M_z|$ and from left to right are 0.2, 0.4, and 0.6. The parameters are $\rho_1 = 1.0$, $\rho_2 = 1.0$, $v_1 = 0.3$, $v_2 = 0.2$, and $k_c = 10$.

$$K_2(\omega) - K_2(0) = \begin{cases} iC\omega & (\omega \ll 2|M_z|), \\ D\pi M_z + iDM_z \ln \left| \frac{1 + \frac{2k_c v_1}{\omega}}{1 - \frac{2k_c v_1}{\omega}} \right| & (2|M_z| \ll \omega \ll x(k_c)), \end{cases} \quad (11)$$

$$A = \frac{2v_1 v_2 (3v_2^2 - v_1^2) - ((v_1^2 + v_2^2)^2 - 4v_1^2 v_2^2) \ln \left| \frac{v_1 - v_2}{v_1 + v_2} \right|}{32v_1^3 v_2^3 / \rho_1},$$

$$B = \frac{v_2 \rho_1}{8\pi v_1^2},$$

$$C = \frac{v_2 \rho_2}{4\pi} \frac{-2v_1 v_2 + v_2^2 \ln \left| \frac{v_1 + v_2}{v_1 - v_2} \right|}{8v_1^2 v_2^2},$$

$$D = -\frac{v_2 \rho_2}{8\pi} \frac{v_2}{v_1^3 - v_1 v_2^2}, \quad (12)$$

where $x(k_c) = \sqrt{M_z^2 + k_c^2(v_1 + v_2)^2} + \sqrt{M_z^2 + k_c^2(v_1 - v_2)^2}$ and k_c is a cutoff value. Equations (10) and (11) show that $K_1(\omega)$ and $K_2(\omega)$ have two frequency regions with different behaviors. The numerical results of Eq. (9) are shown in Fig. 2, and they reproduce the approximate analytical solutions obtained in each region well. Both $K_1(\omega) - K_1(0)$ and $K_2(\omega) - K_2(0)$ reflect the energy dispersion of the MFs. In particular, there are abrupt changes in the values in panels (a), (b), and (c) of Fig. 2, which are the points at $\omega = 2|M_z|$ when the frequency is equal to the band gap. On the other hand, (d) shows a diagram corresponding to the result of the principal value integration in Eq. (9), and there is no peak structure even at $\omega = 2|M_z|$ where the density of states becomes finite.

TABLE I. Electromagnetic degrees of freedom of the double MKPs. They emerge on the surface with WG symmetry when the bulk pair potential belongs to irrep Δ . The magnetization M_z perpendicular to the surface and strain $u_{ij}(\mathbf{x})$, which couple to MKPs, are also shown. The last column denotes that the strain can couple to the double MKPs and to the spin current generated by the same strain. We adapt the definitions for WGs and irreps given by the Bilbao Crystallographic Server [36].

WG	Δ	Magnetization M_z	Strain (spin current)	
			$u_{xx} - u_{yy} (j_y^x + j_x^y)$	$u_{xy} + u_{yx} (j_x^x - j_y^y)$
$p4m$	A_2	Gapped	○	○
$p31m$	A_1	Gapless	\times , only coupled to $u_{xy} - u_{yx} (j_x^x + j_y^y)$	
$p4g$	B_1	Gapped	\times , coupled to $u_{xy} - u_{yx} (j_x^x + j_y^y)$	○

This occurs because the chemical potential of MFs is exactly zero, and $K_2(\omega) - K_2(0)$ is the quantity that can take a finite value when the dispersion of MFs exhibits an energy gap with applied magnetization. Hence, the contribution from the Fermi sea is considered to be dominant.

We emphasize that the electromagnetic multipoles formed by double MKPs determine the properties of the spin current responses to dynamic strains. To see this, by using the results of the previous study [31], we show the general results of couplable strains and the resulting surface spin currents in Table I, which depend on the crystalline and superconducting symmetries of the system (see the Supplemental Material of Ref. [31] for the complete version). The case of $p4m$ corresponds to the present model. In the cases of $p4m$ and $p4g$, the applied magnetization M_z induces an energy gap of double MKPs; however, in the case of $p31m$, the double MKPs remain gapless. In addition, $p4m$ and $p4g$ are both gapped cases, but in the case of $p4g$, the double MKPs do not couple to the strain $u_{xx} - u_{yy}$ but couple to $u_{xy} - u_{yx}$, owing to the protection of the glide-plane symmetry.

In this Letter, we show that a Majorana spin current is generated by spatially nonuniform dynamic strain flows on the surface of a 3D TCSC. For the gapless case, the spin current does not show a damping dependence due to the linear dispersion of the double MKPs and the fact that their chemical potential is exactly zero. In contrast, for the gapped case, the spin currents reflect the energy dispersion of the MFs, and they have a unique frequency dependence. We have shown the application of the general effective theory for the electromagnetic properties of MFs derived from crystalline and superconducting symmetries. Then, one can see the new dynamics of MFs characterized by these symmetries. We believe that our work accelerates the study of the coupling of given external fields with MFs and the transport phenomena arising therefrom.

We suggest that our results can be applied to the surface of the antiperovskite superconductor Sr_3SnO . The antiperovskite A_3BX , $A = \text{Ca, Sr, La}$, $B = \text{Pb, Sn}$, $X = \text{C, N, O}$ with space group symmetry $Pm\bar{3}m$ (No. 221) [37,38], which is equivalent to the O_h PG symmetry, has multiple $J = 3/2$ bands and is a candidate material for topological crystalline insulators due to the band inversion of two orbitals [39–41]. In particular,

Sr_3SnO has the potential to become a TSC with hole doping at temperatures below 5 K [42]. Interestingly, it has been suggested that double MKPs can appear on the (001) surface with $p4m$ WG symmetry when the superconductor symmetry has the A_{1u} representation [43].

As a method of detecting AC spin currents, spin wave resonance can be observed by injecting spin currents into ferromagnetic metals [44,45] and through the rectifying effect of magnetostriction [46]. Dynamic strains $u_{xx}(\mathbf{r}, t)$ and $u_{xy}(\mathbf{r}, t)$ can be realized by a Rayleigh wave and a Love wave propagating in the x direction, respectively. In relation to the experiment, the bulk spin current must not directly arise from inversion-symmetric strains if the bulk has inversion symmetry. This is because a spin current breaks the inversion symmetry but strain does not. Therefore, we suppose that it is experimentally possible to measure only the surface spin current. We also estimate the amplitude of the spin current given by Eqs. (4) and (7). We assume the induced dynamic strain form $u_{xx}(\mathbf{r}, t) = iA_x q_x e^{iq_x r - i\omega t}$, where A_x denotes a lattice displacement, and we set $A_x \sim 0.1 [\text{\AA}]$, $\omega \sim 10^9 [\text{s}^{-1}]$, and $q_x \sim 10^6 [\text{m}^{-1}]$. Additionally, the velocities of MFs are set to $v_1 \sim v_2 \sim 10^4 [\text{m} \cdot \text{s}^{-1}]$ (which is equivalent to the electron velocity in graphene). The coupling energy between MFs and static strain $[u_{xx}]_{\omega=0}$ is given by $E_g = 2|\rho_1 u_{xx}|$, where ρ_1 denotes the coupling constant. We assume that E_g is much smaller than the bulk superconducting gap and set $E_g \sim 0.1 \mu\text{eV}$. Then, $\rho_1 \sim 10^4 \mu\text{eV}$. Therefore, we obtain $|\langle \hat{j}_y^x + \hat{j}_x^y \rangle(\mathbf{r}, t)| \sim 1 \text{ nA}$, where we assume that $\ln[\frac{(v_1 - v_2)^2}{(v_1 + v_2)^2}] \sim 1$ and the system size is $L \sim 1 \text{ mm}$.

The authors gratefully acknowledge M. Matsuo, Y. Nozaki, J. J. Nakane, Y. Imai, T. Yamaguchi, T. Matsushita, R. Kikuchi, and H. Kohno for valuable discussions. Y.Y.'s present affiliation is the RIKEN Cluster for Pioneering Research. This work was supported by JSPS KAKENHI, Grant No. JP20K03835 and the Sumitomo Foundation (190228). Y.Y. is supported by Grant-in-Aid for JSPS Fellows, Grant No. 22J14452. This work was financially supported by JST SPRING, Grant No. JPMJSP2125. The author Y.Y. would like to take this opportunity to thank the ‘‘Interdisciplinary Frontier Next-Generation Researcher Program of the Tokai Higher Education and Research System.’’

- [1] C.-R. Hu, Midgap Surface States as a Novel Signature for $d_{x_a^2-x_b^2}$ -Wave Superconductivity, *Phys. Rev. Lett.* **72**, 1526 (1994).
- [2] S. Kashiwaya and Y. Tanaka, Tunnelling effects on surface bound states in unconventional superconductors, *Rep. Prog. Phys.* **63**, 1641 (2000).
- [3] M. Z. Hasan and C. L. Kane, Colloquium: Topological insulators, *Rev. Mod. Phys.* **82**, 3045 (2010).
- [4] X.-L. Qi and S.-C. Zhang, Topological insulators and superconductors, *Rev. Mod. Phys.* **83**, 1057 (2011).
- [5] Y. Tanaka, M. Sato, and N. Nagaosa, Symmetry and topology in superconductors -odd-frequency pairing and edge states-, *J. Phys. Soc. Jpn.* **81**, 011013 (2012).
- [6] M. Sato and Y. Ando, Topological superconductors: A review, *Rep. Prog. Phys.* **80**, 076501 (2017).
- [7] A. Haim and Y. Oreg, Time-reversal-invariant topological superconductivity in one and two dimensions, *Phys. Rep.* **825**, 1 (2019).
- [8] M. Sato, Y. Takahashi, and S. Fujimoto, Non-Abelian Topological Order in s -Wave Superfluids of Ultracold Fermionic Atoms, *Phys. Rev. Lett.* **103**, 020401 (2009).
- [9] A. Y. Kitaev, Unpaired Majorana fermions in quantum wires, *Phys. Usp.* **44**, 131 (2001).
- [10] R. M. Lutchyn, J. D. Sau, and S. Das Sarma, Majorana Fermions and a Topological Phase Transition in Semiconductor-Superconductor Heterostructures, *Phys. Rev. Lett.* **105**, 077001 (2010).
- [11] Y. Oreg, G. Refael, and F. von Oppen, Helical Liquids and Majorana Bound States in Quantum Wires, *Phys. Rev. Lett.* **105**, 177002 (2010).
- [12] A. Cook and M. Franz, Majorana fermions in a topological-insulator nanowire proximity-coupled to an s -wave superconductor, *Phys. Rev. B* **84**, 201105(R) (2011).
- [13] J. Alicea, New directions in the pursuit of Majorana fermions in solid state systems, *Rep. Prog. Phys.* **75**, 076501 (2012).
- [14] V. Mourik, K. Zuo, S. M. Frolov, S. R. Plissard, E. P. A. M. Bakkers, and L. P. Kouwenhoven, Signatures of Majorana fermions in hybrid superconductor-semiconductor nanowire devices, *Science* **336**, 1003 (2012).
- [15] G. E. Volovik, Fermion zero modes on vortices in chiral superconductors, *JETP Lett.* **70**, 609 (1999).
- [16] N. Read and D. Green, Paired states of fermions in two dimensions with breaking of parity and time-reversal symmetries and the fractional quantum Hall effect, *Phys. Rev. B* **61**, 10267 (2000).
- [17] S. DasSarma, C. Nayak, and S. Tewari, Proposal to stabilize and detect half-quantum vortices in strontium ruthenate thin films: Non-Abelian braiding statistics of vortices in a $p_x + ip_y$ superconductor, *Phys. Rev. B* **73**, 220502(R) (2006).
- [18] L. Fu and C. L. Kane, Superconducting Proximity Effect and Majorana Fermions at the Surface of a Topological Insulator, *Phys. Rev. Lett.* **100**, 096407 (2008).
- [19] C. Nayak, S. H. Simon, A. Stern, M. Freedman, and S. DasSarma, Non-Abelian anyons and topological quantum computation, *Rev. Mod. Phys.* **80**, 1083 (2008).
- [20] D. Aasen, M. Hell, R. V. Mishmash, A. Higginbotham, J. Danon, M. Leijnse, T. S. Jespersen, J. A. Folk, C. M. Marcus, K. Flensberg, and J. Alicea, Milestones Toward Majorana-Based Quantum Computing, *Phys. Rev. X* **6**, 031016 (2016).
- [21] H. Sumiyoshi and S. Fujimoto, Quantum thermal Hall effect in a time-reversal-symmetry-broken topological superconductor in two dimensions: Approach from bulk calculations, *J. Phys. Soc. Jpn.* **82**, 023602 (2013).
- [22] K. Nomura, S. Ryu, A. Furusaki, and N. Nagaosa, Cross-Correlated Responses of Topological Superconductors and Superfluids, *Phys. Rev. Lett.* **108**, 026802 (2012).
- [23] Y. Shimizu, A. Yamakage, and K. Nomura, Quantum thermal Hall effect of Majorana fermions on the surface of superconducting topological insulators, *Phys. Rev. B* **91**, 195139 (2015).
- [24] J. J. He, Y. Tanaka, and N. Nagaosa, Optical Responses of Chiral Majorana Edge States in Two-Dimensional Topological Superconductors, *Phys. Rev. Lett.* **126**, 237002 (2021).
- [25] J. J. He and N. Nagaosa, Local Raman spectroscopy of chiral Majorana edge modes in Kitaev spin liquids and topological superconductors, *Phys. Rev. B* **103**, L241109 (2021).
- [26] T. Tsuneto, Ultrasonic attenuation in superconductors, *Phys. Rev.* **121**, 402 (1961).
- [27] L. P. Kadanoff and I. I. Falko, Ultrasonic attenuation in superconductors containing magnetic impurities, *Phys. Rev.* **136**, A1170 (1964).
- [28] B. Lüthi, Ultrasonics in superconductors, in *Physical Acoustics in the Solid State* (Springer, Berlin, 2005).
- [29] Y. Yamazaki, S. Kobayashi, and A. Yamakage, Magnetic response of Majorana Kramers pairs protected by \mathbb{Z}_2 Invariants, *J. Phys. Soc. Jpn.* **89**, 043703 (2020).
- [30] S. Kobayashi, Y. Yamazaki, A. Yamakage, and M. Sato, Majorana multipole response: General theory and application to wallpaper groups, *Phys. Rev. B* **103**, 224504 (2021).
- [31] Y. Yamazaki, S. Kobayashi, and A. Yamakage, Electric multipoles of double Majorana Kramers pairs, *J. Phys. Soc. Jpn.* **90**, 073701 (2021).
- [32] See Supplemental Material at <http://link.aps.org/supplemental/10.1103/PhysRevB.108.L060505> for I. Effective Hamiltonian on the (001) surface of antiperovskite, II. Spin current induced by dynamic strain.
- [33] T. Funato and M. Matsuo, Acoustic Rashba–Edelstein effect, *J. Magn. Magn. Mater.* **540**, 168436 (2021).
- [34] The impurity effect can be taken into the self-energy by using the self-consistent Born approximation. The vertex corrections also should be calculated to recover the gauge invariance. However, the vertex corrections yield only higher-order terms for the impurities, and hence qualitatively and quantitatively the results do not change. The details of the vertex corrections are shown in Sec. II C of the Supplemental Material.
- [35] K. Ziegler, Robust Transport Properties in Graphene, *Phys. Rev. Lett.* **97**, 266802 (2006).
- [36] L. Elcoro, B. Bradlyn, Z. Wang, M. G. Vergniory, J. Cano, C. Felser, B. A. Bernevig, D. Orobengoa, G. de la Flor, and M. I. Aroyo, Double crystallographic groups and their representations on the Bilbao Crystallographic Server, *J. Appl. Cryst.* **50**, 1457 (2017).
- [37] A. Widera and H. Schäfer, Übergangsformen zwischen zintlphasen und echten salzen: Die verbindungen A3BO (MIT A = Ca, Sr, Ba und B = Sn, Pb), *Mater. Res. Bull.* **15**, 1805 (1980).
- [38] J. Nuss, C. Mühle, K. Hayama, V. Abdolazimi, and H. Takagi, Tilting structures in inverse perovskites, M3TiO (M = Ca, Sr, Ba, Eu; Tt = Si, Ge, Sn, Pb), *Acta Cryst. B* **71**, 300 (2015).

- [39] T. Kariyado and M. Ogata, Three-dimensional dirac electrons at the Fermi energy in cubic inverse perovskites: Ca_3PbO and its family, *J. Phys. Soc. Jpn.* **80**, 083704 (2011).
- [40] T. Kariyado and M. Ogata, Low-energy effective Hamiltonian and the surface states of Ca_3PbO , *J. Phys. Soc. Jpn.* **81**, 064701 (2012).
- [41] T. H. Hsieh, J. Liu, and L. Fu, Topological crystalline insulators and Dirac octets in antiperovskites, *Phys. Rev. B* **90**, 081112(R) (2014).
- [42] M. Oudah, A. Ikeda, J. N. Hausmann, S. Yonezawa, T. Fukumoto, S. Kobayashi, M. Sato, and Y. Maeno, Superconductivity in the antiperovskite Dirac-metal oxide $\text{Sr}_{3-x}\text{SnO}$, *Nat. Commun.* **7**, 13617 (2016).
- [43] T. Kawakami, T. Okamura, S. Kobayashi, and M. Sato, Topological Crystalline Materials of $J = 3/2$ Electrons: Antiperovskites, Dirac Points, and High Winding Topological Superconductivity, *Phys. Rev. X* **8**, 041026 (2018).
- [44] D. Kobayashi, T. Yoshikawa, M. Matsuo, R. Iguchi, S. Maekawa, E. Saitoh, and Y. Nozaki, Spin Current Generation Using a Surface Acoustic Wave Generated via Spin-Rotation Coupling, *Phys. Rev. Lett.* **119**, 077202 (2017).
- [45] S. Tateno, G. Okano, M. Matsuo, and Y. Nozaki, Electrical evaluation of the alternating spin current generated via spin-vorticity coupling, *Phys. Rev. B* **102**, 104406 (2020).
- [46] T. Kawada, T. Funato, H. Kohno, and M. Hayashi, Acoustic spin Hall effect in strong spin-orbit metals, *Sci. Adv.* **7**, eabd9697 (2021).